AAPS PharmSciTech (2022) 23:247
https://doi.org/10.1208/s12249-022-02397-4

RESEARCH ARTICLE

In Situ Forming Chitosan-Alginate Interpolymer Complex Bioplatform for Wound Healing and Regeneration

Hillary Mndlovu[1] · Pradeep Kumar[1] · Lisa C. du Toit[1] · Yahya E. Choonara[1]

Received: 9 May 2022 / Accepted: 10 August 2022 / Published online: 1 September 2022
© The Author(s), under exclusive licence to American Association of Pharmaceutical Scientists 2022

Abstract

Cytocompatibility, biocompatibility, and biodegradability are amongst the most desirable qualities of wound dressings and can be tuned during the bioplatform fabrication steps to enhance wound healing capabilities. A three-stepped approach (partial-crosslinking, freeze-drying, and pulverisation) was employed in fabricating a particulate, partially crosslinked (PC), and transferulic acid (TFA)-loaded chitosan-alginate (CS-Alg) interpolymer complex (IPC) with enhanced wound healing capabilities. The PC TFA-CS-Alg IPC bioplatform displayed fluid uptake of 3102% in 24 h and a stepwise degradation up to 53.5% in 14 days. The PC TFA-CS-Alg bioplatform was used as a bioactive delivery system with an encapsulation efficiency of 65.6%, bioactive loading of 9.4%, burst release of 58.27%, and a steady release of 1.91% per day. PC TFA-CS-Alg displayed a shift in cytocompatibility from slightly cytotoxic (60–90% cell viability) to nontoxic (> 90% cell viability) over a 72-h period in NIH-3T3 cells. The wound closure and histological evaluations of the lesions indicated better wound healing performance in lesions treated with PC TFA-CS-Alg and PC CS-Alg compared to those treated with the commercial product and the control. Application of the particulate bioplatform on the wound via sprinkles, the *in situ* hydrogel formation under fluid exposure, and the accelerated wound healing performances of the bioplatforms make it a good candidate for bioactive delivery system and skin tissue regeneration.

Keywords alginate · chitosan · *in situ* hydrogel · partial crosslinking · wound healing

Introduction

Natural polymers are highly used and attractive compounds in designing wound dressing bioplatforms. Alginate is one of those versatile and attractive polymers owing to its biological properties which include water-solubility, cytocompatibility, biocompatibility, and fluid resorbability [1]. Natural polymers may present a wide range of exceptional properties for wound healing applications. However, their poor mechanical properties limit their individual use in designing wound dressing bioplatforms. For this reason, natural polymers are often combined with synthetic polymers to fabricate bioplatforms with controlled degradation [2].

The use of synthetic polymers in wound dressing has its drawbacks such as toxicity, non-degradable, and not bioresorbable, and they are not as effective in accelerating wound healing or antimicrobial activity [3, 4]. Natural polymers may also present toxicity. However, an optimum combination and processing of natural polymers such as chitosan with calcium alginate have demonstrated efficient healing and pain-relieving in both chronic and acute wounds which include ulcers and burns [5, 6]. Alginate forms an interpolymer complex (IPC) with chitosan via ionic interaction between alginate's carboxylic group and the amine group of chitosan. This interaction allows for the fabrication of various bioplatforms and the loading of bioactives. The biological properties of both alginate and chitosan allow them to be employed in various dressings.

Chitosan is a cationic polymer capable of forming an intermolecular network with anionic polymers and drug molecules. The protonation of the free amine group from $–NH_2$ in alkaline conditions to $–NH_3^+$ in acidic conditions allows for controlled drug release [7, 8]. Apart from the ionic interaction between chitosan and anionic polymers,

✉ Yahya E. Choonara
yahya.choonara@wits.ac.za

[1] Wits Advanced Drug Delivery Platform Research Unit, Department of Pharmacy and Pharmacology, School of Therapeutic Sciences, Faculty of Health Sciences, University of the Witwatersrand, 7 York Road, Parktown, Johannesburg 2193, South Africa

anionic compounds such as trans-4-hydroxy-3-methoxycinnamic acid can also have an ionic interaction with chitosan via the use of the carboxylic group of TFA and the amine groups of chitosan. Furthermore, the hydrophobic property of trans-4-hydroxy-3-methoxycinnamic acid could also facilitate hydrophobic interaction with the hydrophobic chain of chitosan. Trans-4-hydroxy-3-methoxycinnamic acid also known as trans-ferulic acid (TFA) is a ubiquitous phenolic antioxidant, antimicrobial, anti-ageing, anti-diabetic, and anticancer compound predominantly found in the plant cell wall.

TFA antioxidant, antimicrobial, and anti-inflammatory properties allow it to be incorporated in wound dressing bioplatforms. TFA presented a wide range of antimicrobial activities against both Gram-positive and Gram-negative bacteria by facilitating the inhibition of arylamine N-acetyltransferase in the bacteria [9–11]. Cyclooxygenase and nitric oxide synthase function/expression along with the activation of *nuclear factor-kappa-light-chain-enhancer B* cells are inhibited by TFA in both chronic and acute inflammation [12–14]. TFA can easily be used with natural polysaccharides such as chitin and chitosan. This is due to the occurrence of TFA in polysaccharides, glycoproteins, polyamines, lignin, and hydroxylated fatty acids of seeds and leaves [15].

The rapid oxidation tendency of TFA in the environment limits its application in the cosmetic, food, and biomedical field. However, it has been reported that chitosan-based films, nanoparticles, and microparticles with improved matrix characteristics present exceptional incorporation, protection, and controlled release of a variety of compounds including antibiotics, anti-inflammatory, and anti-cancer agents [16]. With the use of chitosan and its properties, TFA could be encapsulated, protected, and released in a controlled manner. A recent study highlighted the effective immobilisation, protection, and release of TFA in microparticles than in nanoparticle bioplatforms [17]. Furthermore, the interaction of TFA and chitosan affected the microparticles and nanoparticles' bioplatform's morphology which improved the bioplatform's anti-fungal activity on growth, spore germination, and morphology of *A. parasiticus* [17]. The hydrophobic character of TFA along with limited solubility in aqueous solution limits TFA's encapsulation, loading, and bioavailability thereby reducing its clinical efficiency. These limitations can be improved by the use of natural-based polymeric bioplatforms as carrier systems and also to increase TFA's solubility, bioavailability, and cytocompatibility.

Bioactive loading and release could also be controlled by introducing crosslinkers and monitoring the degree of crosslinking [18, 19]. The crosslinking of polymers has received much interest in the biomedical field due to improved mechanical properties. Nevertheless, there is still a need to explore and report on the use of partial-crosslinking of alginate and drug-loaded chitosan for wound dressing applications. The ionic character of chitosan allows it to be crosslinked by crosslinkers such as glutaraldehyde and salts such as sodium tripolyphosphate (NaTPP). Several studies indicated efficient fabrication of nano/microparticles and beads by crosslinking chitosan with tripolyphosphate [17, 20]. These drug-loaded bioplatforms can be formed by employing the droplet extrusion method where the drug-loaded chitosan solution is poured drop-wise into sodium TPP aqueous solution [20] or with the ionotropic gelation approach where the chitosan solution is sprayed on the drug-loaded TPP solution [17]. A previous study introduced a novel three-step approach (partial-crosslinking, free-drying, and pulverisation of bioplatforms) in fabricating partially crosslinked bioplatforms with improved physical and mechanical properties [21]. Properties such as porosity, fluid uptake, degradation, visco-elasticity, and cytocompatibility were improved by employing the three-stepped approach [21].

The partial-crosslinking approach made use of salts such as calcium chloride for crosslinking alginate and NaTPP for crosslinking chitosan into beads [21]. The beads and nano/microparticle bioplatforms have been reported to allow for optimum incorporation of antioxidants [16]. However, the incorporation of TFA in bioplatforms has its limitations. Those limitations include TFA's poor solubility and low bioavailability in the body limited by the first-pass metabolism [22]. These limitations led to the exploration of various approaches in an attempt to improve the encapsulation efficiency and release of TFA. These approaches included but not limited to the immobilisation of TFA in, (a) nanoparticles [23], (b) nanostructured lipid carriers and solid lipid nanoparticles [22], and (c) niosomes [24]. Based on these literature data, the conceptualisation of this study and the aim to fabricate cytocompatible, biodegradable, and fluid absorbing drug-loaded biopatform was crafted. The bioplatform would form a hydrogel *in situ* under a fluid environment, thereby presenting optimum TFA release and wound healing performances. The objective of this study was to employ the three-stepped approach in (i) partial-crosslinking alginate and TFA-loaded chitosan, (ii) lyophilization, and (iii) pulverisation of the bioplatforms. It was envisaged that the three-stepped approach would improve the physical and mechanical properties of the bioplatform while the loading of TFA and the biological properties of the two natural polymers will facilitate wound healing performances such as faster wound closure and enhanced tissue regeneration.

Experimental Section

Material

Medium molecular weight chitosan (75–85% deacetylation, 190–300 kDa) was purchased from Sigma-Aldrich

(St. Louis, MO, USA). The calculated degree of deacetylation was 84.36% as obtained using 1H NMR analysis. Chitosan was dissolved in a 1:1 ratio of deuterated acetic acid and deuterated oxide and the analysis was acquired at 70°C. Sodium alginate was procured from Sigma-Aldrich (St. Louis, MO, USA). The calculated mannuronic acid and guluronic acid concentration ratio (A_{1025}/A_{1078}) of 1.51 was obtained via FTIR analyses as described in literature [25]. Glacial acetic acid, calcium chloride, sodium tripolyphosphate, and trans-4-hydroxy-3-methoxycinnamic acid (Trans-Ferulic acid 99%) were purchased from Sigma-Aldrich (St. Louis, MO, USA). Simulated wound fluid constituted of 2% (w/w) bovine serum albumin (BSA), 0.02 M CaCl2, 0.4 M NaCl2, and 0.08 M tris(hydroxymethyl) aminomethane dissolved in deionised water and adjusted to a pH 7.4. A commercial alginate-based wound dressing (Pharma-Algi®, Pharmaplast) was acquired for comparative studies.

Preparation of Partial-Crosslinked Alginate and FA-Loaded Chitosan Micromatrices

Partial-crosslinked alginate (PC Alg) and TFA-loaded chitosan (PC TFA-CS) micromatrices were prepared as described elsewhere [21]. Briefly, chitosan powder was dissolved in a 2% $^{V}/_{V}$ glacial acetic acid aqueous solution to make a final chitosan solution (2% $^{W}/_{V}$) and partially crosslinked (PC) with 2% $^{W}/_{V}$ sodium tripolyphosphate (TPP) solution. A 0.67% $^{W}/_{V}$ TFA solution was prepared in dimethyl sulfoxide (DMSO) solution and mixed with chitosan solution to make a final 0.5% $^{V}/_{V}$ DMSO solution. The partial crosslinking of TFA-CS suspension was achieved by pouring the suspension drop-wise into the 2% $^{W}/_{V}$ TPP solution and the formed TFA-loaded beads were immediately rinsed with distilled water to control the degree of crosslinking. The degree of crosslinking was found to be 40.14% for chitosan and 21.44% for alginate [21]. The rinsed beads were immediately placed in the − 80°C freezer for 24 h, followed by the lyophilization process using the lyophilizer (Free zone 12, Labcono, Kansas City, USA) for 24 h. Using the pestle and mortar, the lyophilized beads were pulverised into micromatrices (< 63 µm). The sodium alginate beads were prepared in the same manner as the chitosan beads. Briefly, a 2% $^{W}/_{V}$ solution of sodium alginate was crosslinked with 2% $^{W}/_{V}$ $CaCl_2$ and rinsed with deionised water before being frozen at − 80°C for 24 h and lyophilized for 24 h. The partially crosslinked alginate beads were also pulverised into micromatrices. The PC-Alg and the PC TFA-CS particles were mixed (1:1 ratio) and sprinkled into simulated wound fluid for the *in situ* formation of the TFA-loaded interpolymer complex (IPC). The formed IPC was allowed to form a gel overnight followed by freeze-drying before characterisation.

Electrical Potential of the Bioplatforms

The nano zeta sizer technique was employed to determine the particle surface charge of PC TFA-CS bioplatform and confirm the interactions between the biomolecules by comparing the shift in the zeta potentials of the crosslinked, uncrosslinked, and TFA-loaded bioplatforms. The zeta potential was evaluated using the Zetasizer Nano ZS instrument (Malvern Instruments (Pty) Ltd., Worcestershire, UK). The prepared PC TFA-CS, PC Alg, and PC TFA-CS-Alg IPC bioplatforms were sonicated in deionised water and filtered before the suspension was transferred into the cell for analysis of the zeta potential at 25°C.

Physicochemical Characterizations of the Bioplatforms

The shifts and changes in the bonds of the main functional groups that were involved in the interactions in the micromatrices were determined using the FTIR spectra of wavelength between 4000 and 650 cm^{-1} at 64 scans using a PerkinElmer Spectrum 2000 ATR-FTIR (PerkinElmer 100, Llantrisant, Wales, UK) spectrometer fitted with a single-reflection diamond MIRTGS detector. Furthermore, the changes in the phase present in the micromatrices were assessed comparatively by recording the X-ray diffraction diffractogram on the benchtop MiniFlex 600 (Rigaku, Japan) diffractometer using CuKα radiation at 40 kV and 15 mA. The 2θ scan range was between 3 and 90° at a scan rate of 10°/min. The thermostability properties of the bioplatforms were followed via the use of the differential scanning calorimeter (DSC) (Mettler Toledo, DSC, STARe System, Swchwerzenback, ZH, Switzerland) and thermo-gravimetric analyser (TGA) (PerkinElmer, TGA 4000, Llantrisant, Wales, UK). The sample preparation of bioplatforms for DSC analysis was as follows, 3 to 10 mg samples sealed in aluminium crucibles and heated over a temperature range of 0 to 400°C at a heating rate of 10°C/min under N_2 atmosphere. DSC curves were plotted as a function of heat flow against temperature. Samples were also prepared for TGA analysis and heated at a rate of 10°C/min from 30 to 900°C under continuous nitrogen purging. Thermograms were generated as percentage weight *versus* temperature.

Surface Morphology Evaluation, Fluid Uptake, and Degradation Analyses

Zeiss sigma scanning electron microscopy (FESEM, 300 VP, ZEISS Research Microscopy Solutions, Jena, Germany) with an accelerating voltage from 10 to 15 kV was employed for the evaluation of the surface morphology of the micromatrices. The micromatrices were mounted on aluminium stubs using carbon adhesive tape and coated

with carbon/gold–palladium in a 2:1 ratio. Fluid uptake and degradation of the bioplatforms were performed under simulated *in vitro* exudative conditions via the use of the orbital shaking incubator (LM-530–2, MRC Laboratory Instruments Ltd. Hahistadrut, Holon, Israel) maintained at 37°C, and set at a speed of 50 rpm as reported in the earlier research report [21]. PC TFA-CS-Alg IPC bioplatform was weighed (50 mg) into vials and PBS 5 mL (pH 7.4) was added. Fluid uptake of the bioplatforms was measured at 1, 2, 4, 8, and 24 h. The fluid uptake was calculated using Eq. 1. The rate of degradation was measured after 1, 3, 7, 10, and 14 days. The degree of degradation was obtained via the use of Eq. 2.

$$\text{FU}\ (\%) = \left(\frac{Mh - Md}{Md}\right)x100 \tag{1}$$

$$\text{Degradation}\ (\%) = \left(\frac{Mo - Md}{Md}\right)x100 \tag{2}$$

where *FU%* is the percentage fluid uptake; *Mo* is the initial dry mass of the sample before being immersed in the fluid; *Mh* and *Md* are the mass of the bioplatforms in the hydrated and dry state, respectively.

Hydrogel Formation Kinetics of PC TFA-CS-Alg IPC

The hydrogel formation and interpolymer complexation were evaluated using the ElastoSens™ Bio2 (Rheolution instruments, Canada). The ElastoSens™BIO2 technique measures in real-time and non-destructively the shear storage (G′) and loss (G″) moduli of hydrogels as a function of time or temperature. The analysis is based on the gentle mechanical vibration of a sample confined in a sample holder and the response is detected by a laser. The real-time *in situ* forming hydrogel kinetics of the IPC were determined by mixing PC Alg and PC TFA-CS in a 1:1 ratio to a total of 100 mg bioplatform mixture and initiated the interpolymer complexation by pouring 3 mL of the SWF into the sample holder at 37°C. The gelling, ionic interaction, fluid absorption, and viscoelastic (G′ and G*) properties of semi-stiff IPC hydrogel were determined over time.

Encapsulation Efficiency (EE), Drug Loading (DL), and *In Vitro* Release Studies

PC TFA-CS-Alg IPC was stirred in SWF pH 7.4 to allow for the complete release of TFA. The bioactive loading and encapsulation efficiency was determined via the use of the standard curve obtained from the measurement of 0, 5, 10, 15, 20, and 25 µg/mL standard solutions of TFA in SWF at the wavelength of 310 nm using UV–Vis nanophotometer (IMPLEN, NP80 NPOS 4.2 built 14,900 UV–Vis nanophotometer, Jena, Germany). The total bioactive to polymer ratio was calculated to obtain the expected amount (mass in milligrammes) of TFA in any given weighed bioplatform amount (mass). The expected TFA amount per bioplatform mass would give insights into the encapsulation efficiency and bioactive loading of the bioplatform via the use of the equations below;

$$\text{EE}\ (\%) = \left(\frac{Mi}{Mf}\right)x100 \tag{3}$$

$$\text{DL}\ (\%) = \left(\frac{Mi}{Mt}\right)x100 \tag{4}$$

where *Mi* is the amount (mass) of drug obtained from the standard curve after complete release, *Mf* is the calculated amount (mass) of TFA in the bioplatform as per the sample preparation method, and *Mt* is the total weighed bioplatform mass used for drug release study. The TFA release study was carried out based on the total mass that the bioplatform can release (Mi) and not the mass from the drug to polymer ratio (*Mf*).

The release study was carried out in 100 mL SWF (pH 7.4) using the Snake Skin dialyses tube (3.5 K MWCO, 22 mm, Thermo Fisher scientific Inc.) diffusion technique maintained at 37°C stirring at 30 rpm in the orbital shaking incubator (LM-530–2, MRC Laboratory Instruments Ltd. Hahistadrut, Holon, Israel) for 72 h. Aliquots (2 mL) were withdrawn at predetermined time points (1, 2, 4, 8, 12, 24, 48, and 72 h) from the release medium and replaced with an equivalent volume of fresh media to maintain sink condition. The amount of the TFA encapsulated in the micromatrice and released at predetermined time points in the SWF medium was determined at 310 nm with UV–Vis nanophotometer. The average absorbance (done in triplicates) of TFA released at the time (*t*) was used in the standard curve to obtain the concentration of TFA released and multiplied by the dilution factor to get the undiluted concentration of released TFA at pre-determined time points. The concentration was divided by the bath volume to get the mass of TFA released at those predetermined time points. The percentage release was obtained by getting the percentage mass fraction of TFA released at time *t* to the amount of TFA that was completely released from the bioplatform (*Mi*) which was represented as *pt*. The cumulative drug release was determined using the formula below as described by Chandrasekaran *et al*. [26];

$$\text{pt} = \left(\frac{Mr}{Mi}\right) X\ 100 \tag{5}$$

$$\text{Cumulative release} = \left(\frac{sample\ volume\ withdrawn}{bath\ volume}\right) X\ p(t-1) + pt \tag{6}$$

where Mr is the amount of drug released at the predetermined time t, pt is the percentage released at time t, and $p(t-1)$ is the percentage released before time t.

In Vitro Cytocompatibility Evaluation of the Bioplatforms

A comparative commercial product, TFA, and PC TFA-CS-Alg were prepared for cell viability tests on the mouse embryonic fibroblast NIH-3T3 cell line. The NIH-3T3 cells were grown in DMEM medium supplemented with 10% FBS and 1% antibiotics. NIH-3T3 cells (100 µL of 1×10^4 cell/mL) were seeded in each 96-well plate and incubated in a humidified chamber overnight at 37°C with an atmosphere containing 5% CO_2. This was followed by adding 1 mg of PC TFA-CS-Alg containing 100 µL DMEM medium per well. This was done in replicates (6 times). The same approach was done for the comparative product (5 mm diameter) and TFA. The cells exposed to samples were incubated in a humidified chamber overnight at 37°C with an atmosphere containing 5% CO_2 for predetermined time points; 24, 48, and 72 h. For positive control, NIH-3T3 cells were maintained with DMEM medium without any additions and for the negative control, the cells were killed with dimethyl sulfoxide (DMSO). Ten microliters of MTT (3-(4,5-dimethyl-2-thiazolyl)-2,5-diphenyl tetrazolium bromide) was added to each well plate after each of the predetermined time points and incubated for 4 h. Thereafter, the medium and the bioplatforms on the well plates were discarded followed by the addition of 100 µL DMSO and incubated overnight on the orbital shaker (at 37°C) to dissolve the formazan. The 96-well plates were measured at an absorbance of 570 nm and 690 nm to subtract the 690 nm absorbance from the 570 nm absorbance to calculate the percentage cell viability on each bioplatforms at the given time points.

In Vivo Wound Closure Performance of the Bioplatforms

In vivo assessment of the wound healing performances of the bioplatforms was followed in a rat model. Female Sprague–Dawley rats (6–8 weeks old) were housed individually, in cages at room temperature (±25°C), maintained under a 12-h light:dark cycle. The animals were fed water and *ad libitum* and allowed to acclimatise to the environment for a week before surgery. The animals were monitored according to the prescribed central animal services (CAS) protocol. All procedures were done in accordance with the Animal Ethics Control Committee of the University of the Witwatersrand animal care regulations following approval by the Animal Ethics Screening Committee of the University of the Witwatersrand (AREC Ethics Clearance No.: 2018/10/49c).

Rats were prepared for punch biopsy surgical procedure by anaesthetizing them with an Isofor and Oxygen gas at a 1:3% mixture and intraperitoneal injection of a 2.7 mL/kg mixture containing midazolam (1.25 mg/mL) and 0.079 mg/mL fentanyl to maintain the rats. The skin over the dorsal area was shaved, and application fields were outlined with a marking pen just before skin excisions. A full-thickness (2-mm thick) wound of 6 mm diameter was created in the dorsal area of the rat by employing the skin punch biopsy apparatus. Using forceps, the skin was lifted in the middle of the wound outline created by the punch biopsy and then the iris scissors (with curved tips) were used to excise the circular piece of tissue. The excised tissue plugs (wound plugs) were fixed in 10% buffered formalin for later processing. A total of two wound areas were created on the dorsal area of each rat. In each group, the rats contained the following treatments on the wound area: untreated (gauze and bandage), comparative product, PC Alg-CS, PC TFA-CS-Alg. The bioplatforms were sterilised with UV before being sprinkled on rats. The dressings were not changed but the bandage was changed weekly. The animals were allowed to heal for 3, 7, 10, and 14 days whereas the wounds were examined, photographed, and excised to measure the reduction in wound size on days 4, 8, 11, and 15 respectively. Wound healing was followed by determining the degree of wound closure (%) given by the size of the wound (measured using the imageJ software) calculated from the following equation.

$$\text{Wound closure (\%)} = \left(\frac{Wound\ area\ day\ 0 - Wound\ area\ day\ t}{Wound\ area\ day\ 0}\right) x\ 100 \quad (7)$$

Histological Analysis

The excised wound plugs at each predetermined wound healing time point allowed for the skin tissues to be stored in 10% formalin for collective evaluation via histopathological analysis. After sufficient fixation of the collected specimens in 10% buffered formalin, the samples were cut according to standard operating procedure (IdexxSA-AP-SOP-26) and processed according to routine histological tissue processing in an automated tissue processor with standard operating procedures IdexxSA-AP-SOP-27. Following tissue processing, sections were cut to 5–6 µm (IdexxSAAP- SOP-30) and the slides produced were stained in an automated haematoxylin and eosin tissue stainer (IdexxSA AP-SOP-205) before histological evaluation. The stained sections of each sample were subsequently examined under a light microscope for analysis. Scoring of the wound morphology was done according to 5 features notably: epithelization, fibroblasts, angiogenesis, epidermal-dermal attachment, and

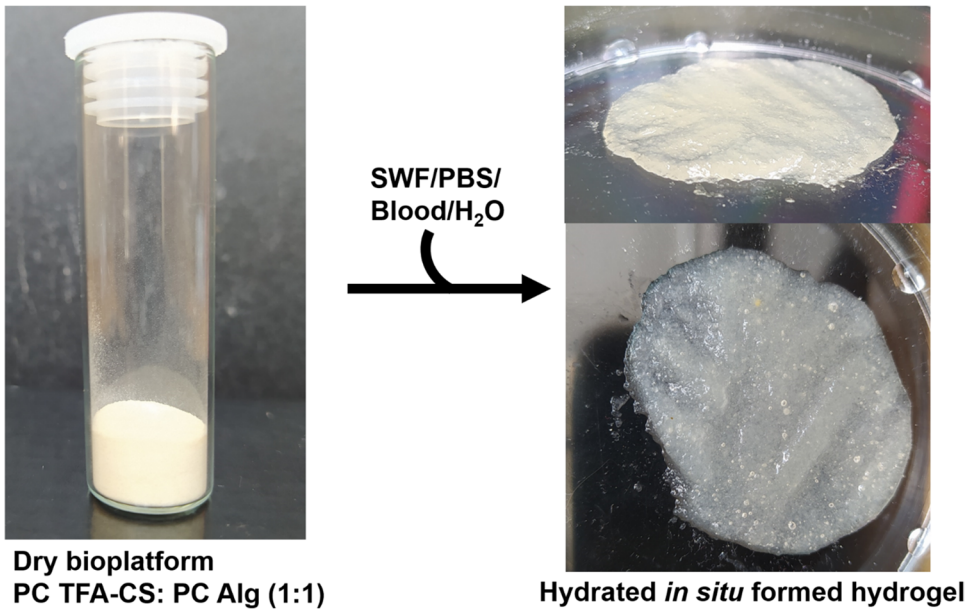

Scheme 1 Hydration of bioplatform to induce *in situ* formation of hydrogel

mononuclear leukocytes. The mode appearance of each bioplatform was used to describe the morphology of the wound plugs.

Results and Discussion

Synthesis of Bioplatforms

The investigations herein, build on earlier research which dealt with the effect of the partial-crosslinking approach on the properties of the bioplatforms. The *in situ* forming hydrogel's structural, physical, and mechanical property transitions were investigated [21]. Herein, the performance of the bioplatforms was investigated in terms of acting as a bioactive delivery system, their cytocompatibility, and in vivo deep-cut wound healing performance. The natural polymers (chitosan and alginate) have been extensively researched in the wound healing field. The performance of these polymers could be enhanced by incorporating bioactives which can improve various properties such as antimicrobial, antioxidant, anti-inflammatory, and wound healing capabilities. Transferulic acid was used in the study owing to its reported anti-oxidative, anti-inflammatory, and antimicrobial properties [11, 13, 14]. Furthermore, the point that TFA is naturally derived makes it an attractive bioactive to be used along with natural polymers for developing wound dressings with multi-properties.

The bioplatforms were synthesised by employing the three-stepped approach, namely partial-crosslinking, freeze-drying, and pulverisation of micromatrices. The percentage of the crosslinkers ($CaCl_2$ and NaTPP) and the polymers (chitosan and alginate) was kept the same at 2%. Bioactives can be incorporated into bioplatforms in various methods such as bulk mixing where the whole bioactive volume/mass is added into polymeric solutions, drop-wise addition of bioactive into a polymeric solution, and coating of a polymeric system in a bioactive solution [27]. In this study, transferulic acid was added drop-wise into chitosan solution to allow for ionic and hydrophobic interactions to form TFA-CS suspension before the crosslinking step. The formed PC TFA-CS was confirmed by observing the zeta potential of the bioplatform against its pristine counterpart. The PC TFA-CS particulate bioplatform was mixed with PC Alg in a 1:1 ratio in simulated wound fluid (pH 7.4) to allow for ionic interaction between the bioplatforms thus facilitating *in situ* hydrogel formation (see Scheme 1).

Zeta Potential of Bioplatforms

Biomolecule surface charge helps in predicting particular interactions between molecules. PC Alg and PC CS were reported to have a highly negative and highly positive zeta potential of -25.8 ± 3.74 and 29.2 ± 5.83 mV, respectively [21]. The high surface charges (zeta potential of $+/-20$ mv) inferred that the partial-crosslinking of chitosan and alginate did not deplete all the polymeric ions. PC TFA-CS ($+20.1$ mv) developed in the current study also showed high surface charges as expected for pristine and partially crosslinked polymers. The slight decrease in the surface charge in the TFA-loaded chitosan suggests that there was ionic interaction between TFA and chitosan. The high surface charge ($+20.1$ mv) in PC TFA-CS allowed for further ionic interaction between PC TFA-CS and PC Alg (-25.8 mV). The point that the zeta potential of PC TFA-CS was below ± 30 mV ($+20.1$ mV) implies that the suspension

was not physically stabilised by electrostatic repulsion [28]. Thus, it could allow for the substitution of TFA with a more ionically stable PC Alg during IPC formation. The high zeta potential of PC TFA-CS, loading of TFA, and the partial-crosslinking of alginate with calcium chloride may contribute to the antibacterial properties of the bioplatform [17, 29–31]. The PC TFA-CS-Alg IPC bioplatform displayed a zeta potential of − 3.58 mV which was indicative of a neutral potential as it was close to zero. The change of zeta potential from both negative and positive intermediate product to neutral potential is suggestive of the ionic interaction that took place between partially crosslinked alginate (− 25.8 mV) and TFA-loaded partial-crosslinked chitosan (+ 20.1 mV) to form the interpolymer complex (− 3.58 mV). These interactions were further assessed via FTIR.

Physical and Chemical Characterisation of Bioplatforms

ATR-FTIR spectroscopy was employed to assess the polymer crosslinking, transferulic acid incorporation, and interpolymer complexation. The TFA FTIR spectrum displayed its phenolic characteristic bands at 3430 cm^{-1}(O–H stretch), 1591 cm^{-1}(C-O stretch), 1460 cm^{-1}(O–H deformation vibration), and 1377 $cm-^{1}$(COO −) (Fig. 1a). These TFA bands correlated with those reported in other studies [32, 33]. There was a disappearance of the characteristic TFA bands in pc TFA-CS at 3430 cm^{-1}, 1662 cm^{-1}, 1460 cm^{-1}, 1202 cm^{-1} which were assigned to O–H stretch, C = O stretch, O–H deformation vibration, and C-O stretch, respectively. The disappearance and shifting of the C-H bands (aromatic) around positions 3078 cm^{-1}, 3018 cm^{-1}, 2970 cm^{-1}, and 2841 cm^{-1} infer that there was also hydrophobic interaction between the aromatic ring of TFA and the chitosan's hydrophobic chains. The additional bands were observed in the spectrum of PC TFA-CS-Alg complex relative to the pristine bioplatforms. FTIR bands shifted while others disappeared in the spectrum of PC TFA-CS-Alg compared to the individual biomolecules (TFA, chitosan, and alginate). This observation was due to both ionic interaction and hydrophobic interaction amongst the two polymers, crosslinkers, and the incorporated TFA. The pristine chitosan amide I band at 1648 cm^{-1} underwent a bathochromic shift to 1598 cm^{-1} in PC TFA-CS followed by a hypsochromic shift to 1648 cm^{-1} in the IPC (PC TFA-CS-Alg). Furthermore, the carboxylic group band at 1538 cm^{-1} in the interpolymer complex can be assigned to C = O bands from both alginate and TFA. Other physical assessments of the bioplatforms were also assessed.

The X-ray diffraction pattern of TFA exhibited characteristic peaks which were also observed in PC TFA-CS. TFA gave characteristic crystalline phases (Fig. 1b). These TFA characteristic peaks were similar to those previously reported in literature [33]. Most diffraction peaks observed for TFA were observed in the XRD diffractogram of PC TFA-CS-Alg IPC except for the TFA peak at 27.32°. The remaining diffraction peaks observed on the PC TFA-CS-Alg IPC were due to the crystalline salts deposited on the surface of the bioplatform as a result of ionic interaction between polymers with respective crosslinkers and the incorporation of TFA ions. The semi-crystalline diffraction pattern of chitosan was still observed along with the TFA crystalline peaks on PC TFA-CS. The PC TFA-CS-Alg IPC exhibited the conserved crystalline peaks observed in PC CS-Alg (Fig. 1b). The presence of TFA diffraction peaks confirmed that TFA was successfully incorporated in the bioplatform, and the presence of calcium salts peaks was indicative of the use of crosslinked alginate on the complex. The diffraction pattern indicative of polymeric amorphous phases was consistent with the one observed on the pristine polymers and the partially crosslinked bioplatforms in terms of following the 110 lattice packing reflection amorphous peaks at 14, 25, and 40° on alginate-based bioplatforms with chitosan having its saccharide peak 11 and 20.5° [21].

Thermo-stability properties of the bioplatforms were also analysed via DSC. The effect of partial-crosslinking on chitosan bioplatforms displayed a conserved dehydration process while exhibiting a shift in the exothermic behaviour from 280 to 240°C on the pristine and partially crosslinked bioplatform, respectively [21]. The TFA endothermic peak at 173°C correlates with the reported 178°C endothermic peak for TFA [33]. The thermal degradation profile of PC TFA-CS was more similar to pristine CS than to PC CS. The endothermic peak at 164°C on PC TFA-CS was a contribution from the melting of TFA incorporated in CS. The PC CS-Alg IPC and PC TFA-CS-Alg bioplatform displayed a conserved melting point at approximately 220 and a degradation process between 240 and 260°C (Fig. 1c). This confirms that the same interpolymer complex had formed and additionally, the sharp endothermic peak at 146°C confirms the incorporation of TFA into the bioplatform.

The DSC assessment of the bioplatforms was accompanied by thermogravimetric analysis (TGA). The incorporation of TFA into the bioplatform decreased the melting point of TFA from 173°C in its pristine form, to 164°C when incorporated in CS followed by partial-crosslinking and finally to 146°C after interpolymer complexation. TFA displayed major degradation (88.24%) from 147 to 165°C while PC TFA-CS exhibited two degradation steps with the first one (8.02% weight loss) from 150 to 200°C and the second one (20%) from 250 to 308°C. The PC TFA-CS-Alg IPC also displayed a two sequential degradation profile with the first one (15.3% weight loss) from 140 to 178°C and the second one (20%) from 250 to 320°C (Fig. 1d). The first step degradation profile of PC TFA-CS and PC TFA-CS-Alg was representative of the degrading TFA in the bioplatforms. The second step degradation profile of PC TFA-CS was due to

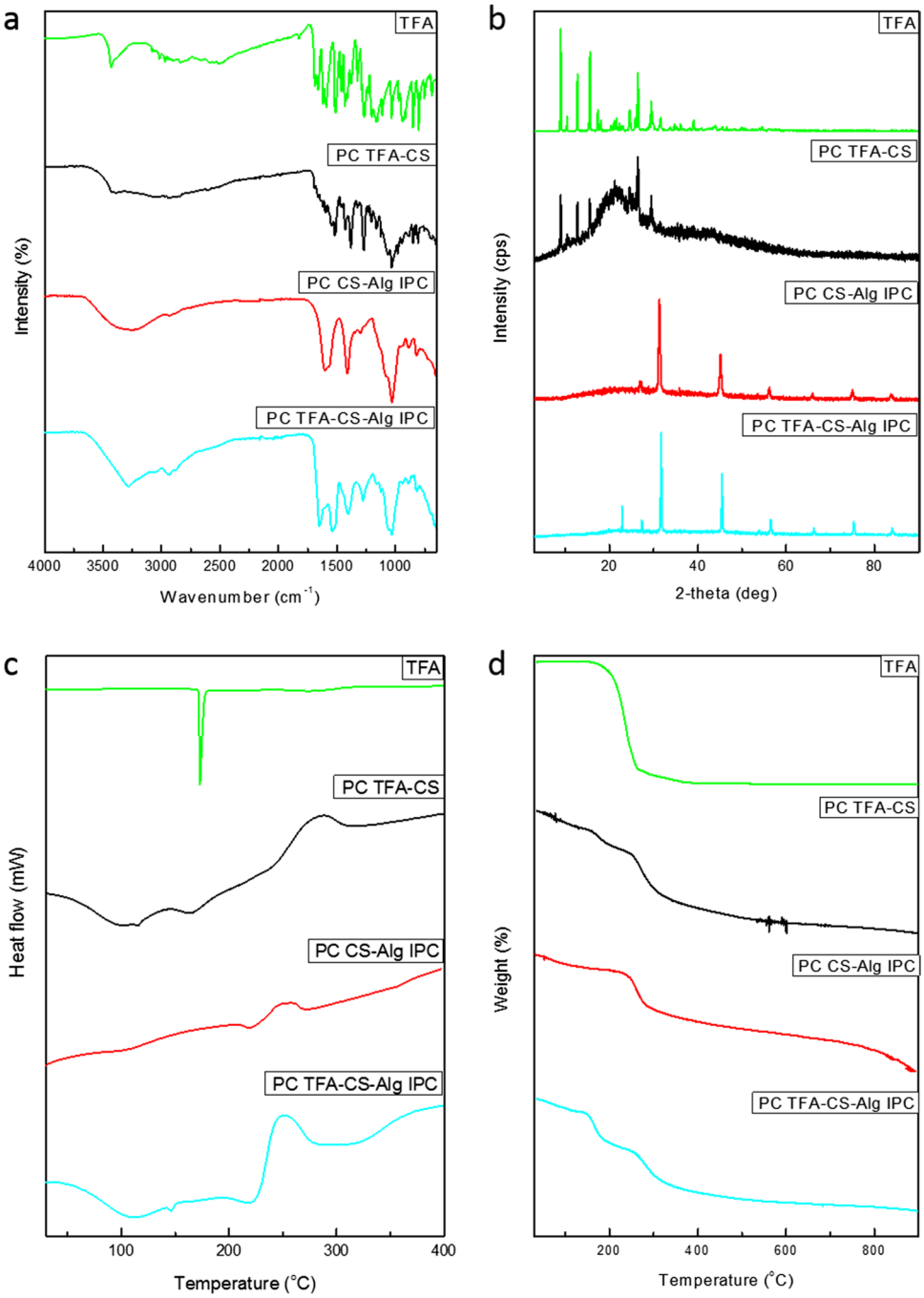

Fig. 1 Functional groups, chemical composition, and phase changes induced by partial crosslinking and TFA loading on the polymers were evaluated via the four analytical techniques **a** FTIR spectra, **b** X-ray diffractograms, **c** DSC, and **d** TGA

the degrading PC CS which correlated with the degradation profile range of PC CS.

Surface Morphology, Fluid Uptake, and Degradation of Bioplatforms

Morphological evaluation of the PC TFA-CS-Alg was undertaken via the use of SEM and the morphological features of PC TFA-CS-Alg did not show particle distribution on the surface as observed in PC CS-Alg. PC TFA-CS-Alg showed curly bundle like structures formed on its surface (Fig. 2ai and ii). PC TFA-CS-Alg also displayed flat surfaces without particles on the surface while other flat surfaces displayed thread-like network structures owing to the interaction of chitosan and alginate which was indicated by the network structures. The network structures were predominantly visible where there were no curly bundle structures (Fig. 2ai and ii). The incorporation of TFA into the IPC reduced the degradation and fluid uptake capacity. The PC CS-Alg (4343.4%) exhibited higher fluid uptake property

compared to PC TFA-CS-Alg in 24 h ([21]. PC TFA-CS-Alg IPC displayed 3102% fluid uptake in 24 h which was maintained for a total of 48 h (Fig. 2b). The high fluid (PBS) uptake could provide a significant fluid absorptive advantage when treating wounds with high volume of exudate and also in case of treating bleeding wounds. The PC TFA-CS-Alg IPC displayed slow stepwise degradation over time with a 53.5% degradation in 14 days (Fig. 2b). This degradation percentage is lower relative to the degradation observed for PC CS-Alg which was 78.2% in 14 days [21]. The high degradation and water uptake capacity of PC CS-Alg IPC infers that the crosslinked TFA-CS complexes induced resistance to degradation of the bioplatform. Although the degradation and fluid uptake of PC TFA-CS-Alg IPC was not the highest amongst the tested bioplatforms, it was still higher than those observed in the comparative product when compared at the same time points (fluid uptake of 1612.56% in 24 h and degradation of 16.26% in 14 days) [21]. The fast fluid uptake by both bioplatforms was crucial for the *in situ* forming hydrogel and the gelling kinetics were subsequently assessed.

Gelling Kinetics of PC TFA-CS-Alg Interpolymer Complex

The ElastoSenseTM Bio2 was used to measure gelling kinetics of PC TFA-CS-Alg IPC. The *in situ* hydrogel formation kinetics were followed via evaluation of the shear storage modulus (G′), loss modulus (G″), complex modulus (G*), and loss tangent (tan θ) as the SWF was mixed with the crosslinked, drug-loaded, and pulverised bioplatforms. The initial increase of the shear storage modulus (G′), loss modulus (G″), and complex modulus (G*) as the SWF was mixed with the crosslinked, drug-loaded, and pulverised

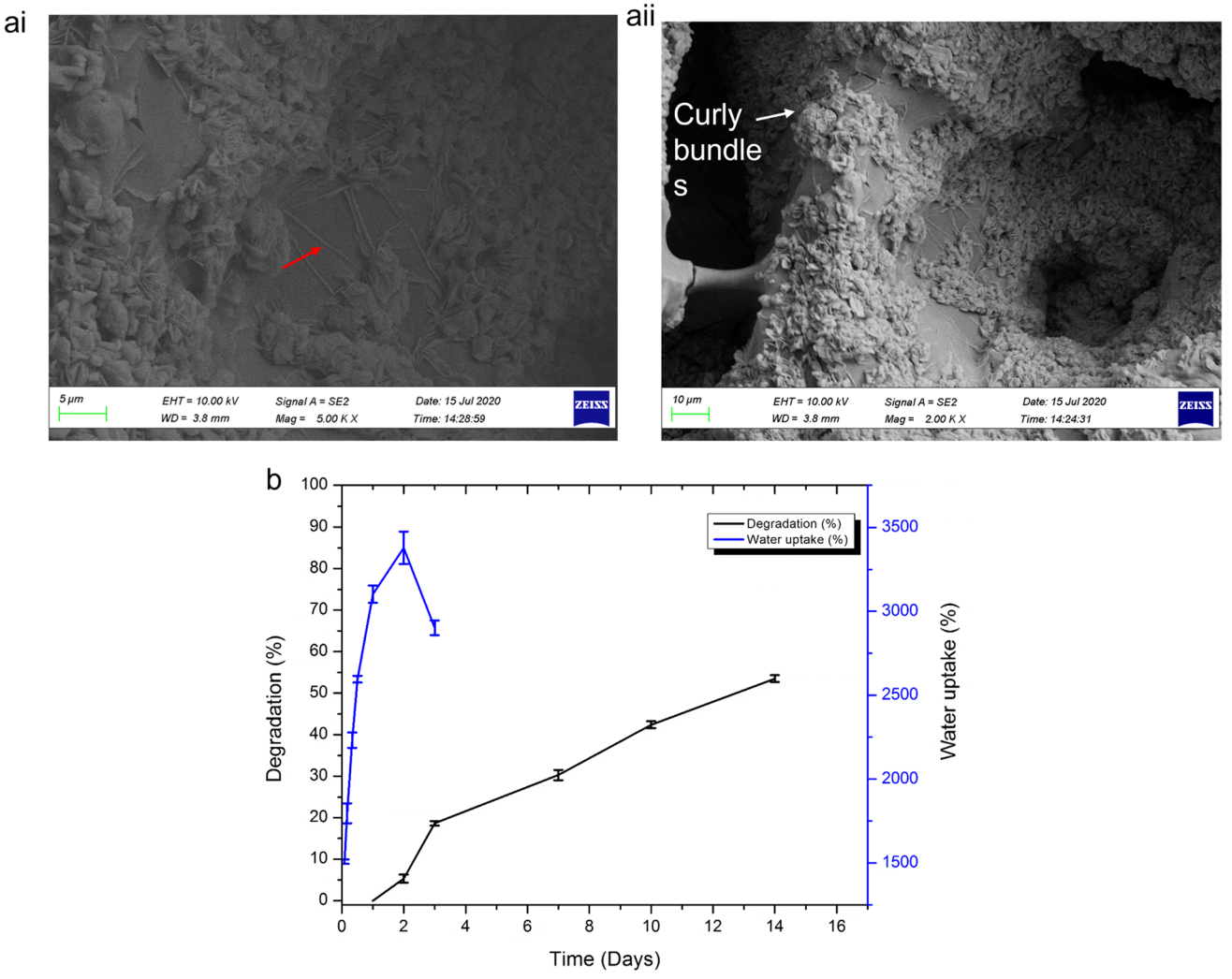

Fig. 2 **a** Morphological evaluation via SEM and **b** fluid uptake capacity and degradation of PC TFA-CS-Alg IPC. Fluid uptake and degradation evaluation were performed in SWF (pH 7.4) solution at 37°C at 50 rpm orbital shaker

bioplatforms was indicative of the *in situ* formation of the IPC hydrogel (Fig. 3). The loss tangent (tan θ) displayed a gradual increase as time proceeded. However, the loss tangent (tan θ) remained under 1. This suggested that both viscoelastic properties were present in the hydrogel. However, the hydrogel tends to be more elastic as the interpolymer complex hydrogel formed [34]. The storage modulus reached the heights of approximately 635 Pa in 5 h which is indicative of the soft nature of the *in situ* formed hydrogel. The formed soft hydrogel may be attributed to the ionic interaction that takes place between polymeric ions at pH 7–8 [35]. The low G′ of the current hydrogel infer that it is softer than the one obtained in the reported work [21]. This suggests that the addition of the TFA on the complex improved the hydrogel in terms of possessing skin mimicking mechanical properties. The skin mechanical properties were reported to vary depending on the depth of the tissues and the following mechanical properties were reported: storage modulus in the stratum corneum (3.787 ± 3.9 MPa and 16.07 ± 2.88 MPa) and further below the VE/dermis junction (3.597 ± 2.35 and 13.977 ± 2.49 MPa) for the 5 μm and 2 μm probe depth, respectively [36].

More assessments on the rigidity (G′) of the formed IPC were followed in different PC Alg to PC TFA-CS ratios and it was observed that the increase in PC TFA-CS amount increased the rigidity of the complex (Fig. 3b). The 7:3 PC TFA-CS to PC Alg ratio resulted in the highest rigidity compared to the 9:1 PC TFA-CS: PC Alg ratio (Fig. 3b

in situ interpolymer complexation. This was observed on the highly rigid 7:1 ratio. The 1:1 ratio displayed controlled rigidity. This ratio would be able to absorb high fluid volumes (such as when bleeding occurs) while maintaining its desirable mechanical properties.

In Vitro Drug Incorporation, Release, and Cytocompatibility Evaluation of the Bioplatforms

UV–Vis absorptive properties of bioactives allow for the assessment of bioactive incorporation and release from bioplatforms. The UV–Vis absorption spectra of the pristine polymers, bioplatforms, and bioactives were evaluated and reported (Fig. 4a). The pristine polymers showed no UV–Vis absorptive properties in the scanned range (200–500 nm). However, partial-crosslinking of alginate introduced UV–Vis absorption properties such as having two peak maxima at 284 and 305 nm. PC CS-Alg also displayed UV absorption properties with two peak maxima at 283 and 305 nm (Fig. 4a). TFA displayed absorption at ~ 230, 286, and 310 nm. The UV absorption of TFA followed in the current study was at 310 nm which correlated with the reported UV–Vis data of ferulic acid having an absorption wavelength (λmax) at 310 nm [37].

TFA was preferably incorporated in chitosan owing to the ionic interaction between the carboxylic parts of TFA with the amine group of chitosan. The encapsulation efficiency and bioactive loading studies were done on the TFA-CS-Alg bioplatform from the mixture of PC TFA-CS and PC Alg in SWF. The *in vitro* release studies were done on the PC TFA-CS-Alg interpolymer complex. The encapsulation efficiency was found to be $65.6 \pm 2.3\%$ and the drug loading was $9.4 \pm 0.51\%$. The bioactive release studies were done under a simulated wound environment (SWF at pH 7.4). The bioplatform showed a burst release of 58% in 8 h followed by a sustained release of 1.91% per day up to a total release of 67.3% in 3 days (Fig. 4b). The encapsulation efficiency and release may seem low. However, TFA has been associated with low encapsulation and release. The literature approaches employed in encapsulating TFA reported TFA encapsulation efficiency of 57.5% [17], encapsulation efficiency of 88.83%, drug loading of 19.9%, coupled with burst release of 20% in 1 h and total release of about 50% in 48 h [23], and in another independent study, a total release of 61% in 1 h [38] was reported. The reported studies have encapsulation efficiency that was below 90%, drug loading that was below 25%, and most of the studies reported drug release that was below 65%. The TFA release profile in this study showed a burst release (58% in 8 h). The 58% TFA release in 8 h would contribute to having a physiological effect as an antioxidant, anti-inflammatory, and antimicrobial agent.

The cytocompatibility of the bioplatforms was evaluated in the *NIH-3T3* cell line over a 72-h period. Given that the burst release was after 8 h, the effect of TFA would also take place from the given time frame. The cytotoxicity of the bioplatform-treated cells was ranked as previously reported by Dahl *et al*., noncytotoxic > 90% cell viability, slightly cytotoxic 60–90% cell viability, moderately cytotoxic 30–59% cell viability, and severely cytotoxic < 30% cell viability [39]. The cytotoxicity ranking of TFA highlighted that TFA-treated cells moved from severely cytotoxic (24% cell viability) to slightly toxic (63% cell viability). However, the increase in the cell viability over the tested period infer that TFA was not highly toxic and cells were able to survive and proliferate daily. The comparative commercial product presented a similar cell viability trend as to that of TFA, with the comparative product having slightly better cell viability in the first 24-h period. Based on the rankings above, the two bioplatforms (PC TFA-CS-Alg and PC CS-Alg) moved from slightly toxic (60–90% cell viability) to nontoxic (> 90% cell viability) over 3 days thus emphasising the cytocompatibility property of the bioplatforms. The slightly lower cell viability of PC TFA-CS-Alg compared to PC CS-Alg may be attributed to the incorporation of TFA on the bioplatform. This was anticipated due to the lower cytocompatibility of

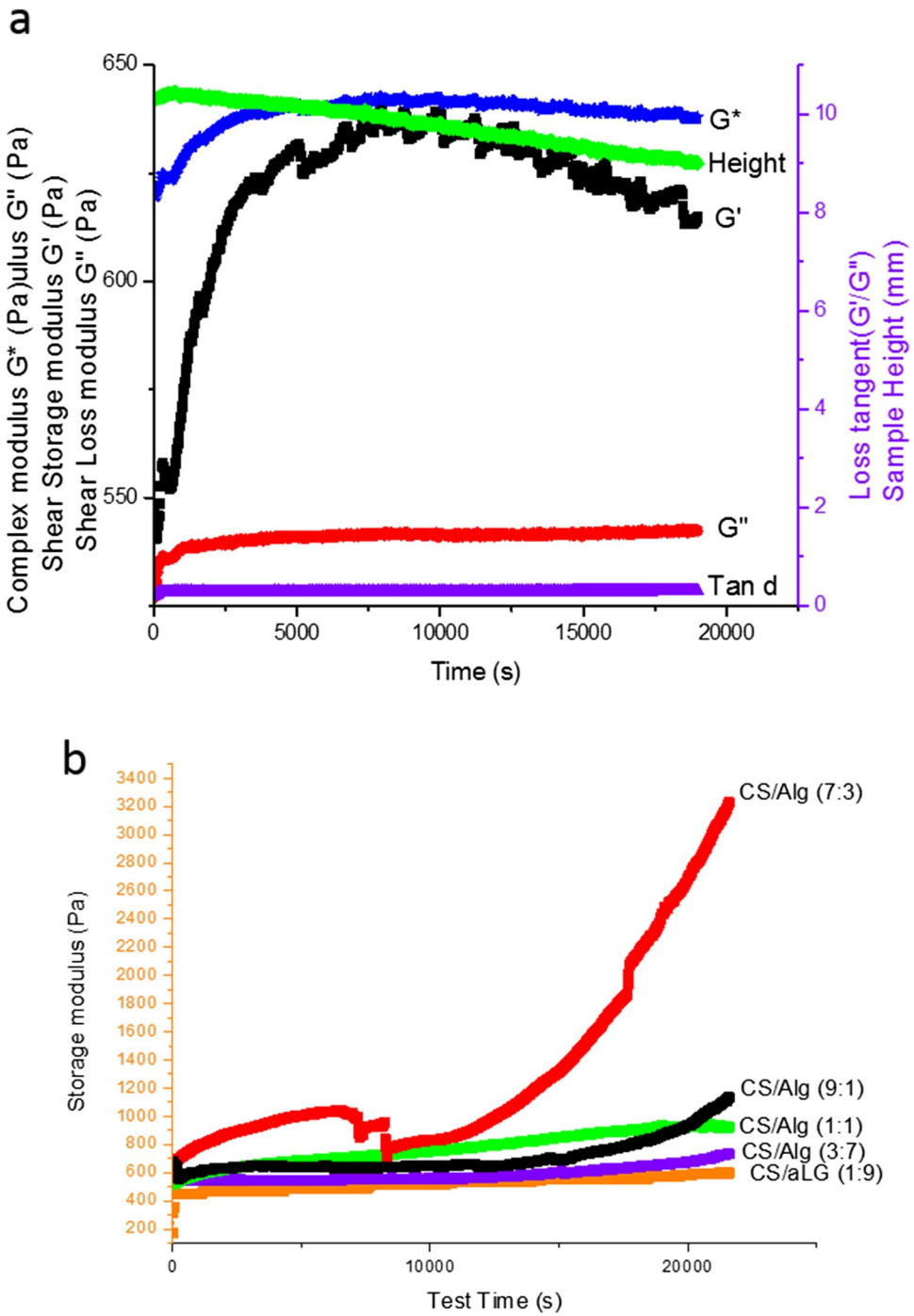

Fig. 3 The hydrogel formation kinetics of PC TFA-CS-Alg in simulated wound fluid (pH 7.4) at 25°C. **a** The interpolymer complex hydrogel was formed *in situ* by mixing PC Alg (50 mg) and PC TFA-CS (50 mg) in 3 mL SWF. The shear storage modulus (gelling and elasticity measurements), shear loss modulus (viscosity), sample height (swelling and absorption functions), shear complex modulus, and loss tangent (viscoelastic properties) were measured in real time. **b** Rate of interpolymer complexation in different bioplatform ratios

TFA evaluated in the study which resulted in the cell viability of 25, 46, and 63% over the 24, 48, and 72 h period, respectively (Fig. 4c). The Bioplatforms tested in the study presented a more favourable environment for optimal cell growth as they all had higher cell viability compared to the comparative product over the 72-h period. The increase in the cell viability on cells treated with the bioplatform was indicative of their cytocompatible nature to facilitate cell growth and potentially wound healing.

Evaluation of *In Vivo* Wound Healing Performance of Bioplatforms

Wound Closure Evaluations of the Bioplatform-Treated Animals

Figure 5 shows the extent of wound closure on lesions in a rat model treated with different bioplatforms. The wounds treated with the same bioplatforms displayed different

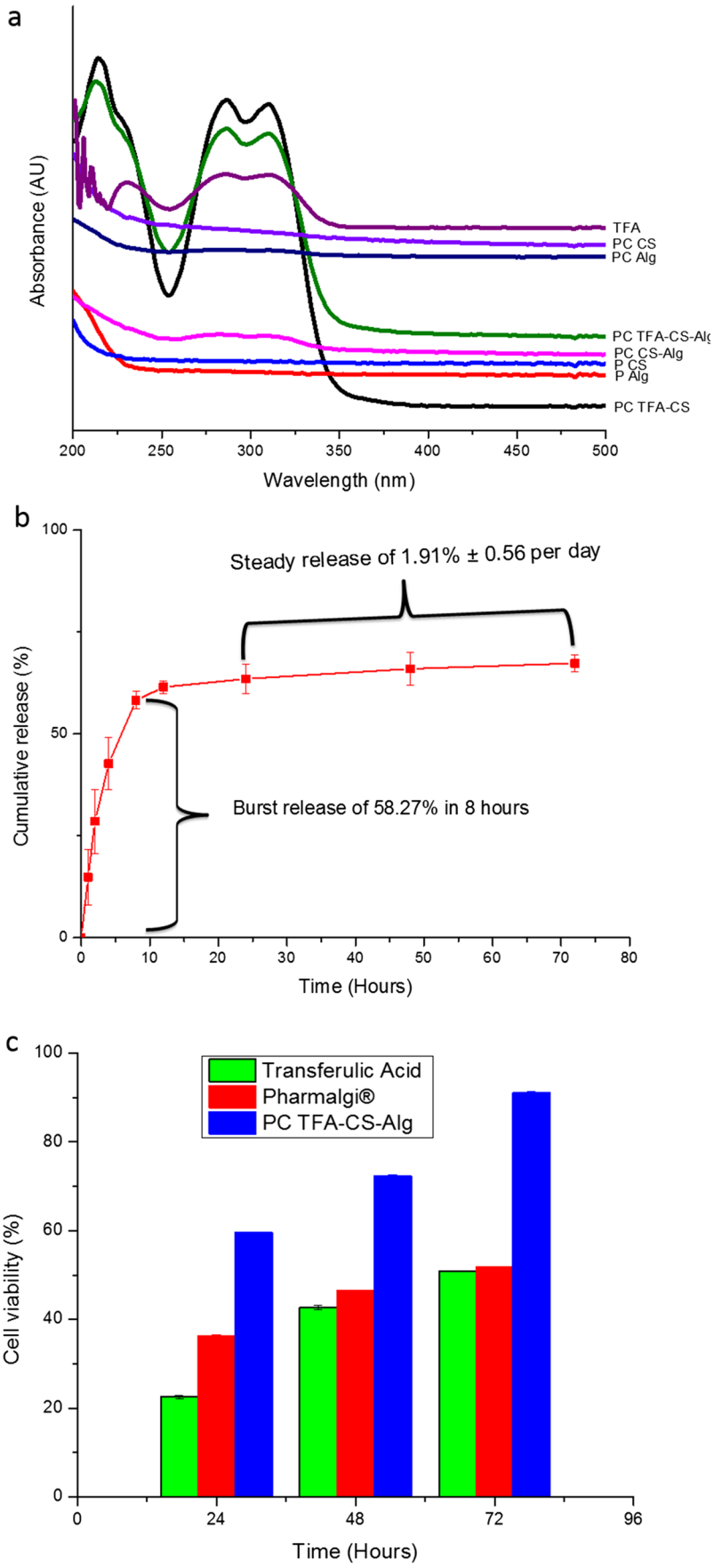

Fig. 4 **a** UV–Vis absorption spectra of the bioplatforms, **b** trans-ferulic acid release from the PC TFA-CS-Alg interpolymer complex in SWF (37°C, pH 7.4) and (C) cell viability assessment of bioplatforms employing MTT assay

wound closure percentages and appearances at the same wound healing time points. Thus, the mode appearance of lesions was used in the figure to describe the overall wound appearance. An average wound closure percentage of each bioplatform at a certain time point was used to get an average wound closure percentage of the wounds.

PC TFA-CS-Alg exhibited accelerated early-stage wound healing performance with more than 30% wound closure after the wounds were allowed for 3 days of wound healing. PC Alg-CS showed the second-highest wound closure rate followed by the commercial product at the same 3-day wound healing period. The wound closure appearance of PC Alg-CS was similar to the wounds treated with PC TFA-CS-Alg. However, the wound closure percentage of PC CS-Alg was close to that of the comparative product–treated lesions. The control group displayed the least wound closure percentage with less than 10% wound closure on day 3. Furthermore, the control lesions appeared fresh compared to the test groups.

All treatment groups displayed more than 70% wound closure by day 7, with the PC TFA-CS-Alg bioplatform having the highest wound closure percentage of 90.45% followed by comparative product (86.62%), PC CS-Alg (85.65%), and lastly the control with 57.7%. PC CS-Alg bioplatform and comparative product displayed similar wound closure percentages over the healing course with the comparative product displaying a slight edge over PC CS-Alg. These wound healing percentages progressed similarly on day 10. All the treatment groups displayed 100% wound closure while the control displayed 98% wound closure after the wounds were allowed to heal for 14 days. Although the wound closure was 100% in the treatment groups, the quality of the healed wounds was different. After 14 days of wound healing, there was no scar tissue or sign of lesion on the site where the wound was created on the animals treated with the PC TFA-CS-Alg bioplatform. The better wound healing property of PC TFA-CS-Alg may be attributed to the following factors but not limited to the TFA antioxidant properties [40] and improved sweeling and mechnanical properties through various fabrication approaches such as using triple hydrophilic polymer system [41] or crosslinking [21].

A bruise-like appearance was observed on the wounds treated with PC CS-Alg bioplatforms. This appearance was also present in the untreated group. Furthermore, the untreated group also showed scar tissues similar to those observed on the lesions treated with the comparative commercial product. The difference in the skin appearance and the absence of scar tissues infer that the wounds treated with PC TFA-CS-TA bioplatform were superior compared to other groups. The differences in the wound appearance were one of the signs of high-quality wound healing performance of the partially crosslinked bioplatforms. The wound remodelling at the epidermis and dermis was further investigated to evaluate the extent and quality of wound healing via histological assessment.

Effect of Respective Bioplatforms on the Lesions (3, 7, 10, and 14 Days)

Automated haematoxylin and eosin (H&E) tissue staining was employed in skin tissues (Fig. 6). This was followed by qualitatively grading lesions on the following five features:

1. Epithelisation which investigated the degree of epithelium covering the original defect in the skin/epidermis [42]
2. Epidermal-dermal attachment which evaluates the epidermal layer advancing along the ulcer/defect surface that is/not adhered/tightly attached to the underlying fibroblastic reaction in the dermis, and this attachment was qualitatively scored [43]
3. Angiogenesis assesses the variable capillaries associated with the dermal and/or subcutaneous fibroblastic reaction [44]. The variability assessment of these capillaries includes specifically arranged patterns typical for granulation tissue (vertical capillaries perpendicular to the skin surface and fibroblasts) mostly in the dermis. In the deeper subcutaneous reaction, they are more haphazardly arranged in the similarly haphazard fibroblastic reaction. They are more prominent in early lesions and become less numerous in more advanced lesions
4. Mononuclear leukocytes are an infiltrate that is not associated with acute exudative inflammation. The inflammation could remain mild in some samples while becoming moderate in areas with endogenous or exogenous foreign material. In the current study, inflammation consisted of varying degrees of mononuclear cells that included lymphocytes, few plasma cells, and macrophages, some of which were epithelioid and multinucleate giant cells
5. Fibroblasts reaction is very important in wound healing as it fills the defect and causes contraction, with the result being complete apposition of the peripheral intact edges of the skin. Fibrosis may involve all layers of the affected skin and may be associated with inflammation or angiogenesis. It may appear as horizontal fibrosis between the edges of the defect in more mature lesions, or haphazard arrangement in less mature lesions. It may appear as granulation tissue when typical accompanying neovascularisation is evident, often beneath areas of ulceration in the dermis. Collagen fibres are associated with the fibroblasts in variable amounts.

Detailed assessments of the above features were done on each of the test groups and compared to the comparative product and the control groups. A normal skin sample at day zero showed that the epidermis, dermis and adnexa, and

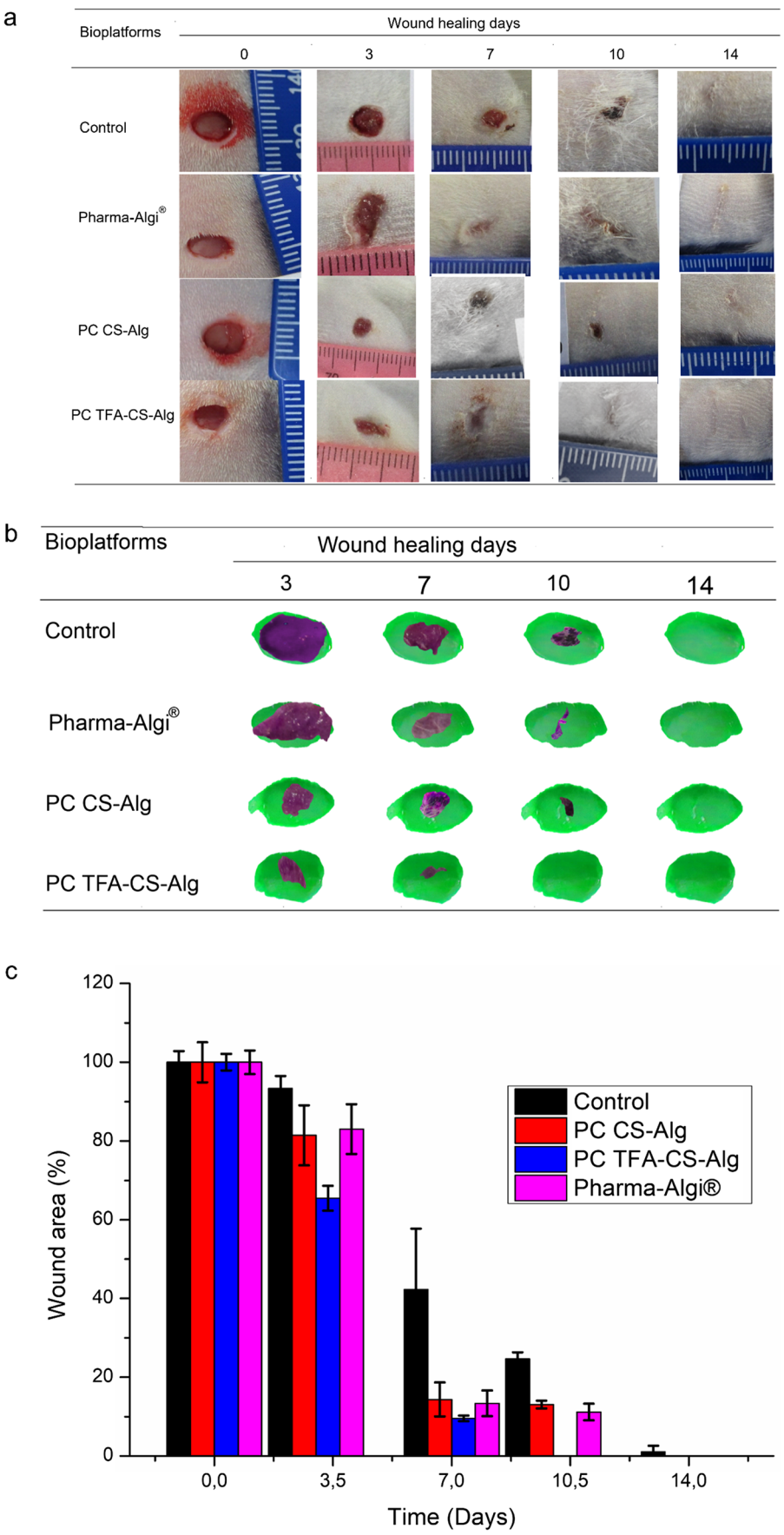

Fig. 5 In vivo representation of the wound healing capabilities of the bioplatforms and commercial comparative product. **a** Wound closure images of SD rats treated with the bioplatforms and allowed to heal over a 14-day period. **b** and **c** are graphical representations of wound closure kinetics of rats treated with bioplatforms

subcutis appeared normal. The underlying muscle layer was intact with a single area showing the presence of large blood vessels penetrating the muscle layer. The features mentioned above were evaluated after each of the wound healing days 3, 7, 10, and 14. Since the bioplatforms displayed different would healing performances on the lesions, the mode characteristics of the wound morphology were used to describe and assess the overall performance of each bioplatform on the lesions in terms of the five features mentioned above.

The early stages of wound healing were evaluated on lesions which were allowed to heal for 3 days. At this early stage of wound healing, all groups did not show any epidermal-dermal attachment. The difference amongst the groups was the collagen deposition which was highest in both PC CS-Alg and PC TFA-CS-Alg-treated lesions followed by the commercial product and the lowest observed in the control group. The wounds treated with PC TFA-CS-Alg displayed a slightly advanced wound healing morphology compared to the ones treated with PC CS-Alg. PC TFA-CS-Alg lesions displayed surface ulceration with marked haemorrhage and fibrin deposition in the ulcer bed whereas the lesions treated with PC Alg-CS displayed severe presence of degenerate neutrophils, a few loose red blood cells, and fibrinous material on the necrotic surface. All groups except for PC TFA-CS-Alg exhibited inflammatory reactions. Fibroblast reaction was more pronounced on the PC TFA-CS-Alg-treated lesions (Fig. 6bii). The lesions treated with the commercial product displayed focally extensive full-thickness epidermal ulceration with mild neutrophilic presence on the ulcerated surface. The untreated/control lesions exhibited loss of the dermal tissues due to similar necrosis present in the subcutis. Focally in the underlying defect in the superficial muscle layer, moderately cellular fibroblastic infiltrates were visible and they appeared haphazardly arranged and accompanied by small numbers of capillaries. The control group displayed further damage in the dermal area whereas the test groups displayed fibroblast reaction taking place at the dermal subcutis. The presence of the fibroblastic reaction in all groups infers that there was tissue regeneration [45]. The fibroblast reaction was high on the partially crosslinked bioplatforms which was indicative of tissue regeneration. The control group displayed further damage in the dermal area whereas the test groups displayed fibroblast reaction taking place at the dermal subcutis. Inflammatory cells were observed in the test groups while it was not visible in the control groups which was a sign that the lesions were exposed to a foreign body [46].

The early-mid wound healing evaluations were made on day 7. At this stage of wound healing, the test groups showed epidermal-dermal attachment whereas the commercial product and control groups displayed unattached epidermal-dermal morphology. The control group was last in the wound healing capabilities with less than 50% wound re-epithelialisation followed by the comparative commercial product groups whereas re-epithelialisation was significant in both test groups PC CS-Alg and PC TFA-CS-Alg. The lack of epidermal-dermal attachment on the control and the comparative product was indicative of inadequate wound healing performances compared to the test groups [43]. The wounds treated with the commercial product displayed central ulceration but surrounding re-epithelialisation from the edges covered approximately 50% of the lesions. The wounds treated with PC CS-Alg and those treated with PC TFA-CS-Alg showed complete covering epidermis which was moderately hyperplastic attached. The test groups showed epidermal-dermal attachment whereas the comparative product and control groups displayed unattached epidermal-dermal morphology. The overall wound healing performance of both test groups was superior to the comparative product and control groups with PC TFA-CS-Alg exhibiting relatively better results than PC CS-Alg at the early-to-mid stages of the wound healing stage. The PC CS-Alg bioplatform displayed more favourable wound healing performance compared to PC TFA-CS-Alg, the comparative product and the control at the mid-late phase of wound healing. The slight wound healing edge of PC CS-Alg at this stage of wound healing may be due to the point that the bioactive (TFA) had already played its part at the early stages of wound healing, and the only contribution to wound healing at this stage was solely on the interaction of the regenerating tissues with polymeric bioplatforms.

The mid-late wound healing evaluations were made after 10 days of wound healing. PC CS-Alg-treated lesions did not show any crusting and also displayed fewer inflammatory cells compared to the control. Serocellular crusting was observed in both PC TFA-CS-Alg and the control group with the control group showing more crusting than PC TFA-CS-Alg. The particulate bioplatforms displayed a more covered ulcerated area compared to both the commercial product and the control. The control (untreated) lesions displayed focal ulceration associated with serocellular crusting in the ulcer bed. The epithelialization and slight epidermal-dermal attachment were more pronounced in the control group compared to the commercial product (Fig. 6bi and iii). However, fibroblast reaction was slightly higher in the commercial product–treated group (Fig. 6bii). The comparative commercial product–treated lesions showed epithelialisation extending from the margins of the defect and covering less than 50% of the ulcerative surface. PC CS-Alg displayed complete re-epithelialisation covering the surface and the mildly hyperplastic epidermis was attached to the underlying dermis throughout. PC TFA-CS-Alg on the other hand displayed ulcerative lesions which were partially covered by epithelium extending from the edges of the wound. PC CS-Alg bioplatform displayed more favourable wound healing

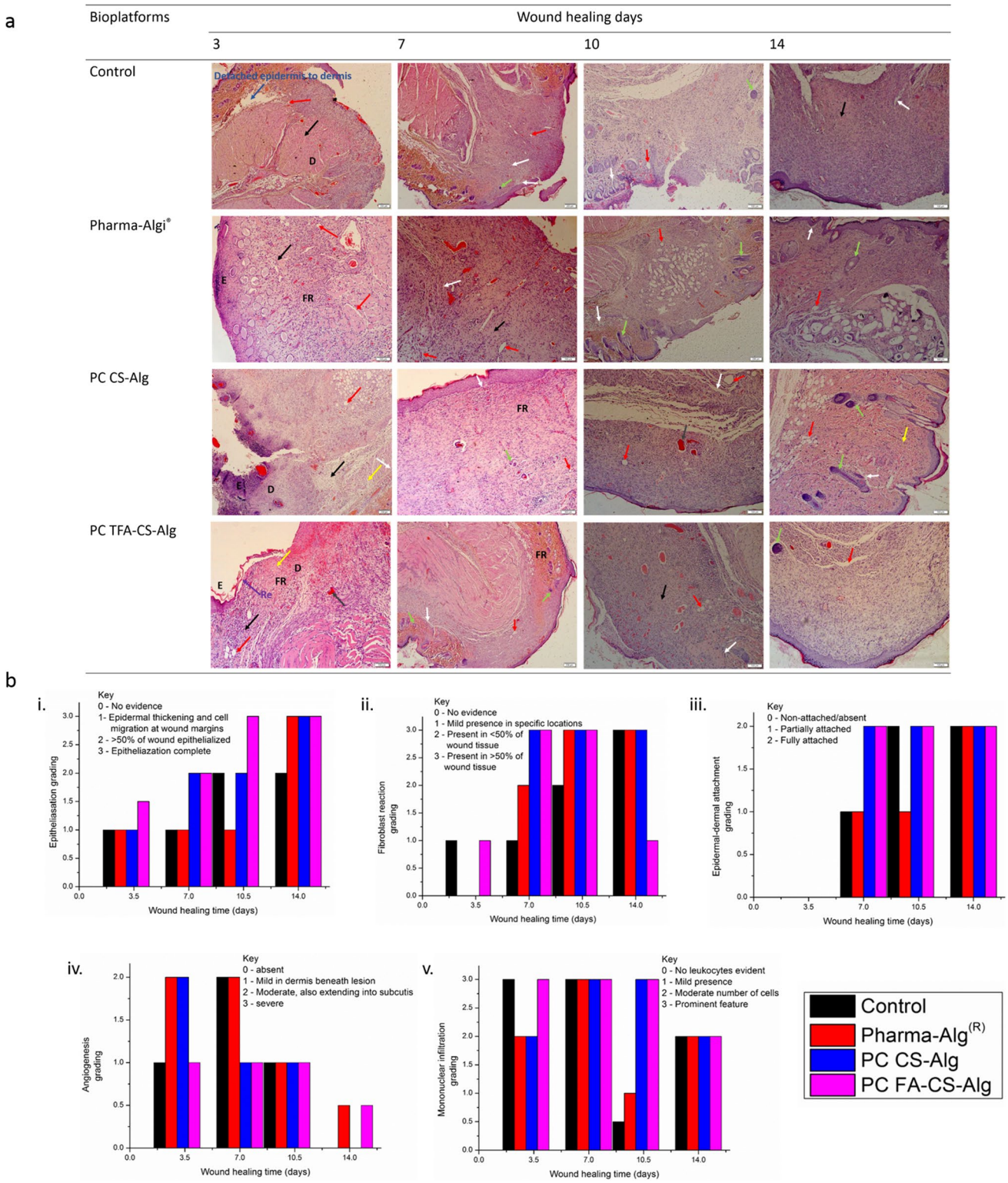

performance compared to PC TFA-CS-Alg, commercial product, and the control.

The late wound healing evaluations were made after 14 days of wound healing. At this stage, all groups displayed similar wound healing performances. The only difference was the quality of the healed tissues which exhibited normal skin morphology in both test groups, the comparative displayed caught up hair follicles, and the control group still indicated horizontal fibroblastic reaction in the dermis causing mild thinning of the dermal

◂**Fig. 6** Early, early-to-mid, mid-to-late, and late wound healing stage of tissues treated with different test groups. **a** The histology of the wound tissues treated with control group, commercial product–treated group, PC Alg-CS-treated group, and the PC TFAC-CS-Alg-treated group. The images were taken at 100× and 200× magnifications. E denotes epidermis development and D represents the dermis layer. FR denotes fibroblast reaction with collagen bundles labelled in yellow arrow, the grey arrow indicates the red blood cells materials, and the purple arrow shows the regenerating edge. The plasma inflammatory cells are indicated by the black arrow, while the blood vessels are indicated by the red arrow and the green arrow indicates hair follicles while the white arrow shows capillaries. **b** Graphical grading of (i) epithelisation, (ii) epidermis-dermis attachment, (iii) angiogenesis, (iv) mononuclear leukocytes, and (v) fibroblastic reaction in the control, scaffolds, and comparative commercial product–treated skin tissues

layer. The mild thinning of the dermal layer extended up to the intact mildly hyperplastic epidermis overlying the wound. Inflammation was more haphazard in the subcutis in the control groups. The commercial product–treated lesions exhibited intact epidermis indicative of complete re-epithelialisation and it appeared to be mildly to moderately hyperplastic. PC CS-Alg bioplatform–treated lesions displayed a completely covered epidermis with minimal hyperplastic and the underlying dermis had a few haphazardly arranged fibroblasts, but normal pilosebaceous units in a regular pattern. The subcutis appeared normal on the PC CS-Alg-treated lesions. PC TFA-CS-Alg-treated lesions also displayed completely covered epidermis with mild hyperplastic and in the underlying dermis, a focal area of horizontal fibrosis becoming slightly haphazard in the deep dermis was observed. There was a thinner dermis in both the control and the comparative group which was evident of inadequate tissue remodelling performance highlighted by thinner collagen fibres characteristic of scar formation in both groups [47]. Furthermore, the control group still indicated inflammation which was indicative of slower wound healing performance relative to the other groups. PC CS-Alg and PC TFA-CS-Alg bioplatform–treated lesions displayed a completely covered epidermis. The subcutis appeared normal on the PC CS-Alg-treated lesions and it was similar to the normal skin tissue observed from day 0. This attests to the high wound-healing quality of PC TFA-CS-Alg. This is supportive of the superiority of the test groups in producing normal skin tissues compared to the control and comparative groups.

Conclusion

The partial crosslinking approach allowed for transferulic acid incorporation in chitosan while maintaining a high-charge potential for further ionic interaction with partial-crosslinked alginate. This approach gives insight into how polymer processing can be explored to fabricate bioactive-loaded interpolymer complexes. TFA incorporation in chitosan and the interpolymer complex was confirmed by both FTIR and Zeta potential. The encapsulation efficiency of TFA was higher than other encapsulation efficiency reported in literature noting the reported difficulties of optimising encapsulation, *in vitro* release, and bioavailability of TFA. The *in situ* forming hydrogel presented both viscoelastic properties which allowed the bioplatforms to absorb wound fluid and remain in the wound cavity while maintaining optimal flexibility. The hydrogel increased loss modulus (G″) while presenting mechanical properties characteristic of a soft hydrogel (G′ below 1 kPa). The bioplatforms' fluid absorption of 3102% in 24 h and stepwise degradation up to 53.5% in 14 days was one of its desirable properties. The bioplatforms were also cytocompatible and cells were able to proliferate in the presence of the bioplatform.

Partial crosslinking along with drug loading drastically improved the cytocompatibility of the bioplatform. The wound closure assessment indicated accelerated wound closure on lesions treated with PC TFA-CS-Alg and a comparable performance between PC CS-Alg and comparative product with the control (gauze) presenting the slowest wound closure capabilities. The histological evaluations of the lesions indicated better wound healing performances in lesions treated with PC TFA-CS-Alg and PC CS-Alg compared to those treated with the commercial product and the control. The accelerated wound healing performance of the bioplatforms was more pronounced at the early stages (day 3) of wound healing with PC TFA-CS-Alg-treated lesions exhibiting a slightly advanced wound healing morphology compared to those treated with PC CS-Alg. The lesions treated with the two bioplatforms presented normal skin tissue morphology compared to the comparative product and the control at the later stages of wound healing. The application of the particulate bioplatform on the wound via sprinkles, the *in situ* hydrogel formation with exudate/fluid absorption properties, and the accelerated wound healing performance of the bioplatforms make it a desirable candidate for use as a drug delivery system and in skin tissue regeneration. The use of polymeric bioplatforms offers an economically vialable option for design and developing future wound dressings given the cost effectiveness of the polymers, ease of storage, and feasible fabrication teachniques.

Acknowledgements Professor Viness Pillay (1970-2020) is hereby kindly acknowledged and remembered for his contributions to the conceptualization of this work.

Author Contribution Hillary Mndlovu: data curation, formal analysis, methodology, roles/writing — original draft, writing — review & editing.

Pradeep Kumar: conceptualization, funding acquisition, investigation, methodology, supervision, validation, visualisation, writing — review & editing.

Lisa C. du Toit: data curation, formal analysis, investigation, methodology, supervision, validation, visualisation, writing — review & editing.

Yahya E. Choonara: conceptualization, funding acquisition, investigation, project administration, resources, supervision, validation, visualisation; writing — review & editing.

Funding This work was supported by the National Research Foundation (NRF) of South Africa; the South African Medical Research Council (SAMRC); and the University of the Witwatersrand, Johannesburg.

Declarations

Conflict of Interest The authors declare no competing interests.

References

1. Sudarsan S, Franklin D, Guhanathan S. Imbibed salts and pH-responsive behaviours of sodium alginate based eco-friendly biopolymeric hydrogels—a solventless approach. Macromol Int J. 2015;11:24–9.
2. Yadav P, Yadav H, Shah VG, Shah G, Dhaka G. Biomedical biopolymers, their origin and evolution in biomedical sciences: a systematic review. J clin diagnos Res: JCDR. 2015;9(9):ZE21.
3. Van den Kerckhove E, Stappaerts K, Boeckx W, Van den Hof B, Monstrey S, Van der Kelen A, *et al*. Silicones in the rehabilitation of burns: a review and overview. Burns. 2001;27(3):205–14.
4. Aderibigbe B, Buyana B. Alginate in Wound Dressings. Pharmaceutics. 2018;10(2):42.
5. Disa JJ, Alizadeh K, Smith JW, Hu Q-y, Cordeiro PG. Evaluation of a combined calcium sodium alginate and bio-occlusive membrane dressing in the management of split-thickness skin graft donor sites. Ann Plastic Surg. 2001;46(4):405–8.
6. Paul W, Sharma CP. Chitosan and alginate wound dressings: a short review. Trends Biomater Artif Organs. 2004;18(1):18–23.
7. Il'ina A, Varlamov V, Ermakov YA, Orlov V, Skryabin K (2008) Chitosan is a natural polymer for constructing nanoparticles. Doklady Chemistry: Springer; 165–7.
8. López-León T, Carvalho E, Seijo B, Ortega-Vinuesa J, Bastos-González D. Physicochemical characterization of chitosan nanoparticles: electrokinetic and stability behavior. J Colloid Interface Sci. 2005;283(2):344–51.
9. Lo H-H, Chung J. The effects of plant phenolics, caffeic acid, chlorogenic acid and ferulic acid on arylamine N-acetyltransferase activities in human gastrointestinal microflora. Anticancer Res. 1999;19(1A):133–9.
10. Tsou M, Hung C, Lu H, Wu L, Chang S, Chang H, *et al*. Effects of caffeic acid, chlorogenic acid and ferulic acid on growth and arylamine N-acetyltransferase activity in Shigella sonnei (group D). Microbios. 2000;101(398):37–46.
11. Borges A, Ferreira C, Saavedra MJ, Simoes M. Antibacterial activity and mode of action of ferulic and gallic acids against pathogenic bacteria. Microb Drug Resist. 2013;19(4):256–65.
12. Hosoda A, Ozaki Y, Kashiwada A, Mutoh M, Wakabayashi K, Mizuno K, *et al*. Syntheses of ferulic acid derivatives and their suppressive effects on cyclooxygenase-2 promoter activity. Bioorg Med Chem. 2002;10(4):1189–96.
13. Nagasaka R, Chotimarkorn C, Shafiqul IM, Hori M, Ozaki H, Ushio H. Anti-inflammatory effects of hydroxycinnamic acid derivatives. Biochem Biophys Res Commun. 2007;358(2):615–9.
14. Batista R (2014) Uses and potential applications of ferulic acid. Ferulic acid: antioxidant properties, uses and potential health benefits 1st ed New York, NY: Nova Science Publishers, Inc 39–70.
15. Smith MM, Hartley RD. Occurrence and nature of ferulic acid substitution of cell-wall polysaccharides in graminaceous plants. Carbohyd Res. 1983;118:65–80.
16. Nair R, Reddy BH, Kumar CA, Kumar KJ. Application of chitosan microspheres as drug carriers: a review. J Pharm Sci Res. 2009;1(2):1.
17. Cota-Arriola O, Plascencia-Jatomea M, Lizardi-Mendoza J, Robles-Sánchez R, Ezquerra-Brauer J, Ruíz-García J, *et al*. Preparation of chitosan matrices with ferulic acid: physicochemical characterization and relationship on the growth of Aspergillus parasiticus. CyTA-Journal of Food. 2017;15(1):65–74.
18. Blüm C, Scheibel T. Control of drug loading and release properties of spider silk sub-microparticles. BioNanoScience. 2012;2(2):67–74.
19. Jeong SH, Park K. Drug loading and release properties of ion-exchange resin complexes as a drug delivery matrix. Int J Pharm. 2008;361(1–2):26–32.
20. Madgulkar A, Bhalekar M, Swami M. In vitro and in vivo studies on chitosan beads of losartan duolite AP143 complex, optimized by using statistical experimental design. AAPS PharmSciTech. 2009;10(3):743.
21. Mndlovu H, du Toit LC, Kumar P, Marimuthu T, Kondiah PP, Choonara YE, *et al*. 2019 Development of a fluid-absorptive alginate-chitosan bioplatform for potential application as a wound dressing. Carbohydrate Polymers 114988.
22. Zhang Y, Li Z, Zhang K, Yang G, Wang Z, Zhao J, *et al*. Ethyl oleate-containing nanostructured lipid carriers improve oral bioavailability of trans-ferulic acid ascompared with conventional solid lipid nanoparticles. Int J Pharm. 2016;511(1):57–64.
23. Bairagi U, Mittal P, Singh J, Mishra B. Preparation, characterization, and in vivo evaluation of nano formulations of ferulic acid in diabetic wound healing. Drug Dev Ind Pharm. 2018;44(11):1783–96.
24. Rezaeiroshan A, Saeedi M, Morteza-Semnani K, Akbari J, Gahsemi M, Nokhodchi A (2020) Development of trans-Ferulic acid niosome: an optimization and an in-vivo study. Journal of Drug Delivery Science and Technology. 101854.
25. Sakugawa K, Ikeda A, Takemura A, Ono H. Simplified method for estimation of composition of alginates by FTIR. J Appl Polym Sci. 2004;93(3):1372–7.
26. Chandrasekaran AR, Jia CY, Theng CS, Muniandy T, Muralidharan S, Dhanaraj SA. Invitro studies and evaluation of metformin marketed tablets-Malaysia. J Appl Pharm Sci. 2011;1(5):214.
27. Mndlovu H, du Toit LC, Kumar P, Choonara YE, Marimuthu T, Kondiah PP, *et al*. Bioplatform fabrication approaches affecting chitosan-based interpolymer complex properties and performance as wound dressings. Molecules. 2020;25(1):222.
28. Müller R, Jacobs C, Kayser O. Nanosuspensions as particulate drug formulations in therapy: rationale for development and what we can expect for the future. Adv Drug Deliv Rev. 2001;47(1):3–19.
29. Hussain F, Khurshid M, Masood R, Ibrahim W. Developing antimicrobial calcium alginate fibres from neem and papaya leaves extract. J Wound Care. 2017;26(12):778–83.
30. Du W-L, Xu Y-L, Xu Z-R, Fan C-L. Preparation, characterization and antibacterial properties against E. coli K88 of chitosan nanoparticle loaded copper ions. Nanotechnology. 2008;19(8):085707.
31. Du W-L, Niu S-S, Xu Y-L, Xu Z-R, Fan C-L. Antibacterial activity of chitosan tripolyphosphate nanoparticles loaded with various metal ions. Carbohyd Polym. 2009;75(3):385–9.
32. Mathew S, Abraham TE. Physico-chemical characterization of starch ferulates of different degrees of substitution. Food Chem. 2007;105(2):579–89.

33. Wang J, Cao Y, Sun B, Wang C. Characterisation of inclusion complex of trans-ferulic acid and hydroxypropyl-β-cyclodextrin. Food Chem. 2011;124(3):1069–75.
34. Moura MJ, Figueiredo MM, Gil MH. Rheological study of genipin cross-linked chitosan hydrogels. Biomacromol. 2007;8(12):3823–9.
35. Rochani A, Agrahari V, Chandra N, Singh ON, McCormick TJ, Doncel GF, *et al*. Development and preclinical investigation of physically cross-linked and ph-sensitive polymeric gels as potential vaginal contraceptives. Polymers. 2022;14(9):1728.
36. Kendall MA, Chong Y-F, Cock A. The mechanical properties of the skin epidermis in relation to targeted gene and drug delivery. Biomaterials. 2007;28(33):4968–77.
37. Pan GX, Thomson CI, Leary GJ. UV–vis. spectroscopic characteristics of ferulic acid and related compounds. J wood Chem Technol. 2002;22(2–3):137–46.
38. Trombino S, Ferrarelli T, Cassano R. A New Pro-Prodrug Aminoacid-Based for Trans-Ferulic Acid and Silybin Intestinal Release. J Function Biomater. 2014;5(3):99–110.
39. Dahl JE, Frangou-Polyzois MJ, Polyzois GL. In vitro biocompatibility of denture relining materials. Gerodontology. 2006;23(1):17–22.
40. Varela-Garcia A, Concheiro A, Alvarez-Lorenzo C. Cytosine-functionalized bioinspired hydrogels for ocular delivery of antioxidant transferulic acid. Biomater Sci. 2020;8(4):1171–80.
41. Jin SG, Kim KS, Kim DW, Kim DS, Seo YG, Go TG, *et al*. Development of a novel sodium fusidate-loaded triple polymer hydrogel wound dressing: mechanical properties and effects on wound repair. Int J Pharm. 2016;497(1–2):114–22.
42. Pastar I, Stojadinovic O, Yin NC, Ramirez H, Nusbaum AG, Sawaya A, *et al*. Epithelialization in wound healing: a comprehensive review. Adv Wound Care. 2014;3(7):445–64.
43. Nishiyama T, Amano S, Tsunenaga M, Kadoya K, Takeda A, Adachi E, *et al*. The importance of laminin 5 in the dermal–epidermal basement membrane. J Dermatol Sci. 2000;24:S51–9.
44. Velnar T, Gradisnik L. Tissue augmentation in wound healing: the role of endothelial and epithelial cells. Medical Archives. 2018;72(6):444.
45. McDougall S, Dallon J, Sherratt J, Maini P. Fibroblast migration and collagen deposition during dermal wound healing: mathematical modelling and clinical implications. Philos Trans Royal Soc A: Math, Phys Eng Sci. 1843;2006(364):1385–405.
46. Coleman D, King R, Andrade J. The foreign body reaction: a chronic inflammatory response. J Biomed Mater Res. 1974;8(5):199–211.
47. Dale PD, Sherratt JA, Maini PK. A mathematical model for collagen fibre formation during foetal and adult dermal wound healing. Proc R Soc Lond B. 1996;263(1370):653–60.

Publisher's Note Springer Nature remains neutral with regard to jurisdictional claims in published maps and institutional affiliations.

Springer Nature or its licensor holds exclusive rights to this article under a publishing agreement with the author(s) or other rightsholder(s); author self-archiving of the accepted manuscript version of this article is solely governed by the terms of such publishing agreement and applicable law.